



## ORIGINAL PAPER

## AN IMPROVED STACKING FILTERING FOR EXTRACTING THE COMMON-MODE ERRORS ON GNSS COORDINATE TIME SERIES IN SHANXI

Wei LI<sup>1, 2, 3, 4)</sup>, Xiaotong LI<sup>1, 2, 3)</sup>\*, Jianfei ZANG<sup>5)</sup>, Zhemin SUI<sup>1, 2, 3)</sup>, Chuang SONG<sup>6)</sup>, Xukang XIE<sup>1, 2, 3)</sup>, Yutong HUANG<sup>1, 2, 3)</sup>, Tengxu ZHANG<sup>7)</sup> and Haowen YAN<sup>1, 2, 3)</sup><sup>1)</sup> Faculty of Geomatics, Lanzhou Jiaotong University, Lanzhou, Gansu 730070, China<sup>2)</sup> National-Local Joint Engineering Research Center of Technologies and Applications for National Geographic State Monitoring, Lanzhou, Gansu 730070, China<sup>3)</sup> Gansu Provincial Engineering Laboratory for National Geographic State Monitoring, Lanzhou, Gansu 730070, China<sup>4)</sup> Faculty of Geo-Information Science and Earth Observation, University of Twente, Enschede 7514 AE, Netherlands<sup>5)</sup> College of Oceanography and Space Informatics, China University of Petroleum, Qingdao 266580, China<sup>6)</sup> School of Engineering, Newcastle University, Newcastle upon Tyne NE1 7RU, UK<sup>7)</sup> College of Resources and Environmental Science and Engineering, Hubei University of Science and Technology, Xianning, Hubei 437100, China

\*Corresponding author's e-mail: 11200854@stu.lzjtu.edu.cn

## ARTICLE INFO

## Article history:

Received 1 November 2022

Accepted 6 December 2022

Available online 16 December 2022

## Keywords:

GNSS station coordinate time series;

Common-mode error;

Stacking filtering;

Environmental loading;

Noise analysis

## ABSTRACT

The presence of common mode error (CME) in the coordinate displacement time series of the Global Navigation Satellite System (GNSS) affects geophysical studies using GNSS observations. In order to investigate the effect of CME on the time series in GNSS networks in Shanxi, this paper proposes an improved superposition filtering method by introducing single-day solution accuracy, correlation coefficient, and spherical distance between stations as weights. The filtering effect is evaluated using the GNSS data in Shanxi. By using the improved stacking filtering method, the root mean square (RMS) values for N, E, U are reduced by approximately 27.8 %, 29.0 %, and 46.0 %, respectively. And compared to the traditional stacking filter, our improved method can achieve better results with CME extraction. We investigate the CME spatial-temporal characteristics and its relationship with environmental loading. The results show that the CME between stations decreases as the distance between stations increases. In addition, we analyze the effect of CME on the noise component and velocity estimates. Results show that removing the CME refines the velocity and leads to a significant reduction in the magnitude of noise, indicating that the CME is dominated by the flicker noise in Shanxi Province.

## 1. INTRODUCTION

Since establishing the Crustal Movement Observation Network of China (CMONOC), a large amount of observational data has been accumulated, including coordinate time series data of continuously operating reference stations (Li et al., 2012; Hein, 2020; Zhou et al., 2022). The coordinate time series are defined as a set of coordinates of a reference station arranged in chronological order. Currently, coordinate time series and their products have been applied to various fields, such as geodetic, earth science, and atmospheric science. In combination with other spatial geodetic tools (such as very long baseline interferometry and satellite laser ranging), these fields can be used to establish and maintain global or regional coordinate reference frames and provide applications for geodesy (Dmitrieva et al., 2015; Altamimi et al., 2016; Jiang et al., 2016, 2018; Ding et al., 2019; Qiu et al., 2022). The horizontal and vertical linear velocities estimated from coordinate time series can be used to study geodynamic phenomena such as plate motion and post-ice rebound (Xu et al., 2010; Trubienko et al., 2013; Yadav et al., 2013; Bogusz et

al., 2019; Lu et al., 2022; Yang et al., 2022). Combining coordinate time series with altimetric satellite and tide gauge station observations can be used to monitor global sea level height changes (Ming et al., 2017). The coupling between monsoon climate and drought can be studied by combining vertical displacement data and precipitable water from reference stations (Jiang et al., 2017). The seasonal signal and geophysical signals from the coordinate time series can be used to study the role of large-scale atmospheric and hydrological mass loads on the elastic Earth and the effects of the mass load on the Earth (Barani et al., 2021).

The GNSS coordinate time series are subjected to a variety of errors, for example, Wdowinski et al. (1997) found a spatially correlated error in the coordinate time series, known as common mode error (CME) in their analysis of the Southern California GPS network coordinate time series. Many researchers have analyzed the sources of CME. Sheng et al. (2014) identified terrestrial water loading as the main component causing CME in the Sichuan and Yunnan regions. Yuan et al. (2013) pointed out that

surface mass loading could explain about 3 mm of the vertical annual variation in the CME series of 12 stations in the Hong Kong region. The presence of CME tends to obscure the internal motion characteristics of the reference station, which in turn affects the accurate and reliable estimation of the position and velocity of the reference station (Dong et al., 2006; Fernandes et al., 2020). By analyzing the time series of approximately 7 years of observations in the Canary Islands, Arnoso et al. (2020) showed that extracting the CME from the time series of each station can effectively improve the signal-to-noise ratio to retrieve high-precision geodetic velocities. Yuan et al. (2013) also presented this conclusion after analyzing the coordinate time series of 12 continuously operating reference stations in Hong Kong.

In recent years, researchers have proposed various methods to extract CME, mainly including principal component analysis (Jackson and Yong, 2004; Abdi et al., 2010; Ji and Herring, 2013; He et al., 2015, 2017a, 2019; Zhou et al., 2018; Li et al., 2020; Tan et al., 2020), Karhunen-Loeve (KLE) expansion (Dong et al., 2006), independent component analysis (Ming et al., 2017), and stacking filter method. Among them, the stacking filtering method is one of the effective methods to extract CME (Bian et al., 2021). Wdowinski et al. (1997) proposed the extraction of CME using the regional superimposed filtering method and pointed out that the application of this method is premised on the assumption that the CME is uniformly distributed in the regional network. The limitation of this method is that it cannot accurately reflect the spatial response among the CME of each station, and the extraction effect weakens as the spatial extent increases. Nikolaidis (2002) considered the single-day solution accuracy of each station when extracting the CME, but ignored the correlation between stations. Scripps Orbit and Permanent Array Center (SOPAC) divided the whole network into several sub-regions in order to accurately extract the CME in the Plate Boundary Observation (PBO) network, and performs superimposed filtering on each sub-region separately. However, this method lacks the basis of regional division and the CMEs at the junction of sub-regions vary greatly (Tian and Shen, 2016).

The traditional stacking filtering method is suitable for observation networks with approximately uniform distribution of CME, while ignoring the fact that the "commonality" of the CME decreases as the spatial extent increases. Therefore, its extraction effect is greatly influenced by the number of stations and spatial distribution. This research proposes an improved superposition filtering method by introducing single-day solution accuracy, the correlation coefficient and the spherical distance between stations as weights. The topography of Shanxi is complex, but it can still be clearly divided into three main parts: the eastern mountainous region,

the western mountainous region and the central basin, fertilizing it a good testing ground for studying the crustal movements. However, some studies have only considered the effect of noise terms in the time domain when extracting regional geophysical signals, without considering CME in the spatial domain (Zhang et al., 2012; Cheng et al., 2021; Sui et al., 2022). Therefore, we use the raw coordinate time series data provided by the GNSS data products of China Earthquake Administration (<ftp.cgps.ac.cn>) for eight continuous observation reference stations in Shanxi province from 2016 to 2020. We fit and remove the trend terms and periodic terms in the raw coordinate time series data to obtain the residual time series, and then use the improved stacking filter method proposed in this research for CME extraction. We also carry out spatial characterization of the extracted CME and study the effect of environmental loading on CME. Finally, the noise and velocity of the time series before and after the elimination of CME is analyzed, providing references for future researches on regional deformation monitoring in Shanxi Province.

## 2. DATA AND METHODS

### 2.1. DATA

CMONOC has accumulated a large amount of time series. 10 stations were set up in the region of Shanxi Province, China, and due to the high level of missing data at SXCH and SXCZ, we selected eight stations (SXDT, SXGX, SXKL, SXLF, SXLQ, SXTY, SXXX, and SXYC) for the study after selection (the location of stations is shown in Figure 1).

The CMONOC time series data used in this paper are from the GNSS Data Product Service Center of the China Earthquake Administration (<data.earthquake.cn>), and the processing software used for its data interpretation is GAMIT/GLOBK (Zhou et al., 2018), developed by Massachusetts Institute of Technology (MIT) (Herring et al., 2010), as used in the solution for geodetic measurements (Li, 2021). It takes into account the effects of various factors such as tides, atmospheric loading and nutation, and considers earth orientation parameter (EOP) in adjustment estimation, enabling highly accurate baseline solutions to be obtained (Herring, 2003; Herring et al., 2010; Iqbal et al., 2021). As the CMONOC time series data were already tidally corrected at the GAMIT data processing, in the study of the effect of environmental load on the common mode error, we chose the non-tidal atmospheric loading (NTAL), non-tidal oceanic loading (NTOL) and the hydrological loading (HYDL) of the global hydrological model LSDM from the Helmholtz Centre-Potsdam-German Research Centre for Geosciences (GFZ, <http://esmdata.gfz-potsdam>) to work out the effects of environmental loading on the CME (Information of environmental loading is in Table 1).

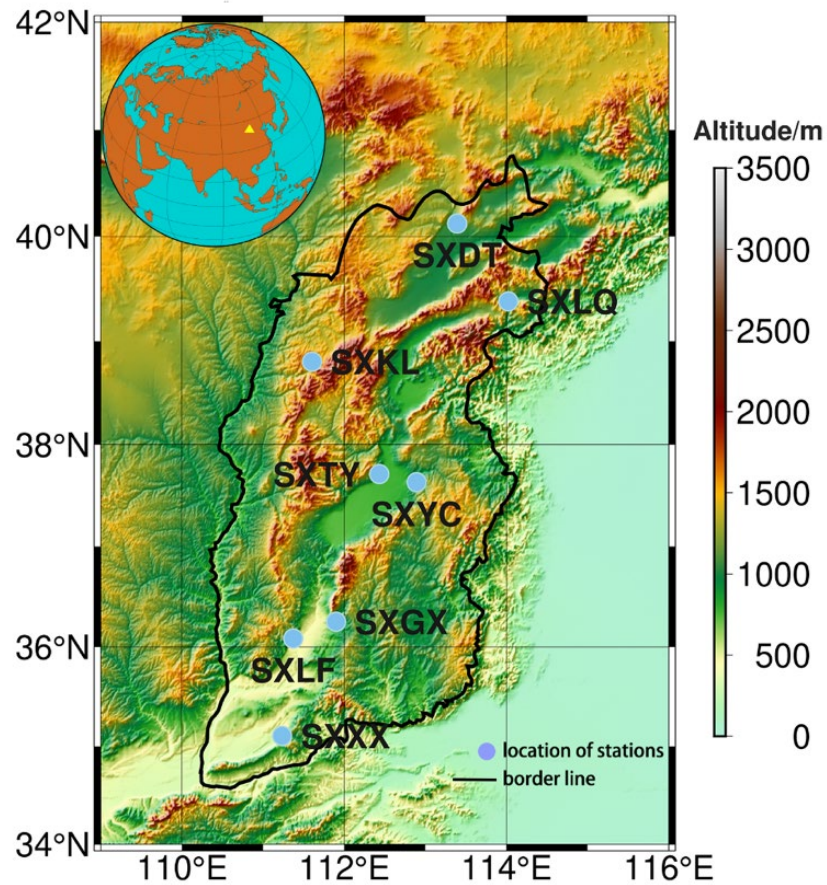


Fig. 1 Distribution of CMONOC stations in Shanxi.

Table 1 Environmental loading product provided by GFZ.

Organizations	Type Model	Spatiotemporal	Resolution	Time Span
GFZ	NTAL	ECMWF	0.5×0.5/3h	1976-present
	NTOL	EMPIOM	0.5×0.5/3h	1976-present
	HYDL	LSDM	0.5×0.5/24h	1976-present

2.2. METHODS

After obtaining the raw time series from these GNSS stations, the time series need to be pre-processed with outlier elimination, step term correction, interpolation and least squares fitting to remove the trend and period terms (annual and semi-annual). In this paper, outlier elimination is carried out using the interquartile range method (Bos et al., 2013), interpolation of missing values is carried out using GMIS software (Liu et al., 2018), and least squares fitting is used to remove the periodic and trend terms from the original time series to obtain the residual time series for subsequent CME extraction. The exact flow of this paper can be seen in Figure 2.

2.2.1. FITTING OF THE TIME SERIES

Before extracting the CME, it is necessary to obtain the residual time series of each station by fitting

the raw time series of each station with least squares (Blewitt and Lavallée, 2002; Jiang et al., 2016). The fitting model considering the period and trend terms is:

$$v_i = y(t_i) - \alpha - b \cdot t_i - c \cdot \sin(2\pi t_i) - d \cdot \cos(2\pi t_i) - e \cdot \sin(4\pi t_i) - f \cdot \cos(4\pi t_i) - H(t_i) \quad (1)$$

where,  $v_i$  represents the residuals between the observed and modelled time series;  $y(t_i)$  is the time series of station coordinates;  $t_i$  represents the solved calendar element in years;  $\alpha$  is the initial coordinates of the station;  $b$  is the linear rate;  $c$  and  $d$  are the coefficients of the annual cycle term;  $e$  and  $f$  are the coefficients of the semi-annual cycle term;  $H(t_i)$  represents the Heaviside step function. A least square fit of the raw time series by the above equation yields the base data for subsequent extraction of the CME.

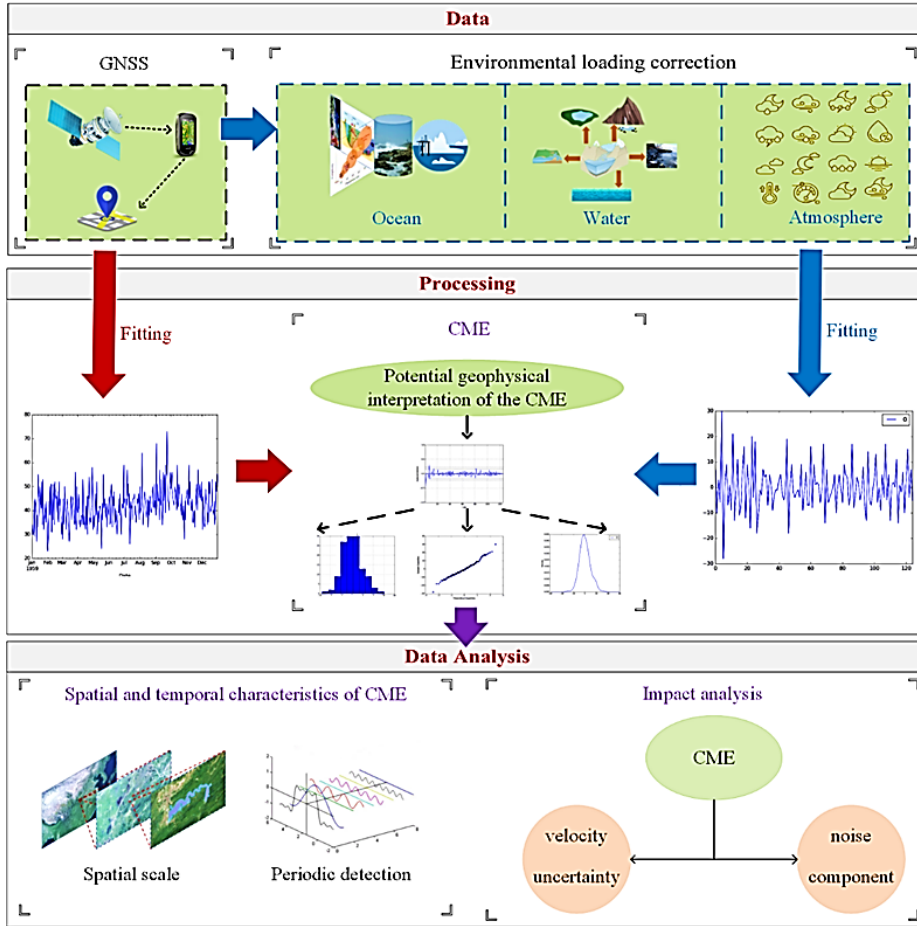


Fig. 2 The flow of this paper.

### 2.2.2. IMPROVED STACKING FILTERING

Stacking filtering is a weighted average algorithm for small-scale observation networks with uniform CME distribution, as a widely used method for CME extraction. Wdowinski et al. (1997) first proposed the use of stacked filtering to extract the CME in time series, which defined the CME value  $\varepsilon(k, i)$  for the  $k$ th station on the  $i$ th day as:

$$\varepsilon(k, i) = \frac{\sum_{k=1}^S v_{k,i}}{S} \quad (2)$$

where,  $S$  is the number of stations in the network participating in the CME extraction;  $v_{k,i}$  is the residual of the position for the  $k$ th station on the  $i$ th day, when  $S = 1$ , the CME is the residual series of this station. On the basis, Nikolaidis (2002) took the single-day solution accuracy into account, and defined the CME as:

$$\varepsilon(k, i) = \frac{\sum_{k=1}^S \frac{v_{k,i}}{\sigma_{k,i}^2}}{\sum_{k=1}^S \frac{1}{\sigma_{k,i}^2}} \quad (3)$$

where,  $\sigma_{k,i}^2$  is the standard deviation of the  $k$ th station on the  $i$ th day.

The above traditional regional stacking filtering methods are applied with the assumption that the CME is uniform in a certain region and are suitable for the case where the CME of GNSS stations is approximately homogeneous. When the spatial extent of the GNSS network increases, the commonality of stations will decrease, which limits the use of these methods. Through experiments, we found that to achieve a better extraction effect, different weighting factors can be introduced in different directions. Therefore, we propose an improved filtering method, through preliminary data analysis, we found that the common mode error is best extracted by introducing the correlation coefficients, distance factors and single-day solution accuracy in the E direction, and correlation coefficients and distance factors in the N and U directions. Our method defines the CME  $\varepsilon(j, i)$  in the E direction for  $i$ th day of the  $j$  station as:

$$\varepsilon(j, i) = \frac{\sum_{k=1}^S \frac{v_{k,i} \cdot \gamma_{j,k}}{\sigma_{k,i}^2 \cdot d_{j,k}}}{\sum_{k=1}^S \frac{\gamma_{j,k}}{\sigma_{k,i}^2 \cdot d_{j,k}}} \quad (4)$$

And the CME  $\varepsilon(j, i)$  in the N and U directions is defined as

$$\varepsilon(j, i) = \frac{\sum_{k=1}^S \frac{v_{k,i} \cdot \gamma_{j,k}}{d_{j,k}}}{\sum_{k=1}^S \frac{\gamma_{j,k}}{d_{j,k}}} \quad (5)$$

where,  $v_{k,i}$  is the residual value of the  $k$ th station on the  $i$ th day;  $\sigma_{k,i}^2$  is the standard deviation of the  $k$ th station on the  $i$ th day; the spherical distance factor  $d_{j,k}$  between station  $j$  and station  $k$  is defined as:

$$d_{j,k} = R \times \arccos[\cos \beta_1 \cos \beta_2 \cos(\alpha_1 - \alpha_2) + \sin \beta_1 \sin \beta_2] \quad (6)$$

where,  $\beta_1$  is the latitude angle of station  $j$ ,  $\alpha_1$  is the longitude angle;  $\beta_2$  is the latitude angle of station  $k$ ,  $\alpha_2$  is the longitude angle;  $R$  is the radius of the earth, taken as 6378.13 km.  $\gamma_{j,k}$  is the correlation coefficient between station  $j$  and station  $k$ , which is calculated as follows:

$$\gamma_{j,k} = \frac{\sum_{i=1}^n (v_{j,i} - \bar{v}_j) \cdot (v_{k,i} - \bar{v}_k)}{\sqrt{\sum_{i=1}^n (v_{j,i} - \bar{v}_j)^2 \cdot \sum_{i=1}^n (v_{k,i} - \bar{v}_k)^2}} \quad (7)$$

### 2.2.3. SPECTRAL INDEX ESTIMATION

The noise of many phenomena in nature has a power-law property, meaning that the power spectral density of the noise is related to the frequency of the noise in a power series (Bos et al., 2013), that is:

$$P(f) = P_0 \left(\frac{f}{f_0}\right)^\alpha \quad (4)$$

where,  $P(f)$  means the power spectral density,  $f$  stands for the frequency of the noise,  $f_0$  is the frequency at normality in the time series, and  $\alpha$  means the spectral index. For noise, the different spectral indices represent different noise characteristics. The spectral indices of most noise in nature are concentrated in the range of  $[-3, 1]$ , where white noise corresponds to a spectral index of  $\alpha = 1$ , flicker noise of  $\alpha = -1$ , and Random Walk Noise (RWN) of  $\alpha = -2$ . For noise with a spectral index between  $[-1, 0]$ , it can be described by the white noise (WN) + flicker noise (FN) model (Langbein, 2004, 2012; Montillet et al., 2012), from which it can be seen that obtaining the spectral index is the key to the determination of the noise model.

### 2.2.4. BAYESIAN INFORMATION CRITERIA (BIC) ANALYSIS

The spectral index estimation method can only roughly estimate the optimal noise model based on the interval in which the spectral index is located. In order to determine the optimal noise model more accurately, this paper uses Hector software (Bos et al., 2013), which is faster in data processing in terms of noise analysis. The following five combinations of noise models provided by Hector are used: (i) White noise (WN), (ii) Power-law noise (PL) + White noise (WN), (iii) Flicker noise (FN) + White noise (WN), (iv) Generalised Gaussian Markov noise (GGM) + White

noise (WN) and (v) Random walk noise (RWN) + Flicker noise (FN) + White noise (WN). This software uses the Bayesian information criterion to select the best model, considers the log-likelihood as a starting point and adds parameters to increase the penalty to avoid overfitting. The log-likelihood function (Bos et al., 2013) is defined as:

$$\ln(L) = -0.5[\ln(\det C) + \hat{v}^T C^{-1} \hat{v} + N \ln(2\pi)] \quad (5)$$

where,  $\det C$  represents the determinant of covariance matrix  $C$ ,  $N$  is the length of the time series and  $\hat{v}$  is the residuals time series after trend fitting. The Bayesian Information Criterion (BIC) is defined as:

$$BIC = k \ln(N) + 2 \ln(L) \quad (6)$$

The number of parameters  $k$  is the sum of parameters in the design matrix and the noise models and the variance of the driving white noise process. For instance, estimating a linear trend using the power-law + white noise model consists of five parameters: nominal bias, linear trend, distribution of variances between power-law and white noise, spectral index of the power-law and the variance of the driving white noise process ( $k = 2 + 2 + 1 = 5$ ). The smaller the value of BIC means the chosen noise model is better, and vice versa.

## 3. RESULTS

### 3.1. TIME SERIES OF GNSS STATION COORDINATES RESIDUALS

In this study, the CMONOC time series data used are from the GNSS Data Product Service Center of the China Earthquake Administration. The residual time series of each station can be obtained by fitting the time series using Equation (1) in Section 2.2.1. Taking the station SXYC as an example, the raw time series and the residual time series of this station are given in Figure 3 (other stations are in Figure S2-S15), it can be seen that there are obvious periodic and trend terms in the raw time series, which are effectively eliminated after the least squares fitting. From the residual time series, we can see that the amplitudes of N and E are small, within  $\pm 5$  mm, while the amplitude of U is larger and can reach  $\pm 20$  mm, this multiplicative relationship is consistent with White et al. (2022). Tregoning and Watson (2009) explain that the horizontal deformation is smaller because the station is subject to multiple loading in the horizontal direction from the surrounding area, resulting in the station being pulled in different directions at the same time.

### 3.2. EXTRACTION OF CME

There is a significant regional common component of CME in the continuous GPS positions based on the global reference frame, which cannot be removed in the stage of GPS raw data processing due to its unknown origin so it is usually eliminated in the

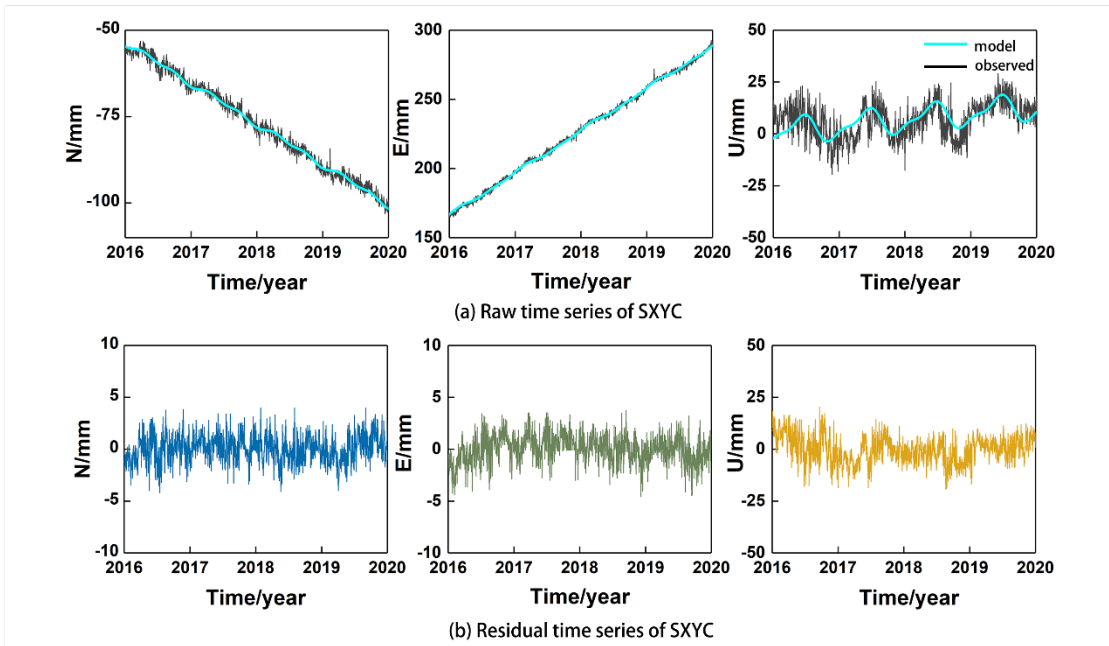


Fig. 3 Raw and residual time series of SXYC.

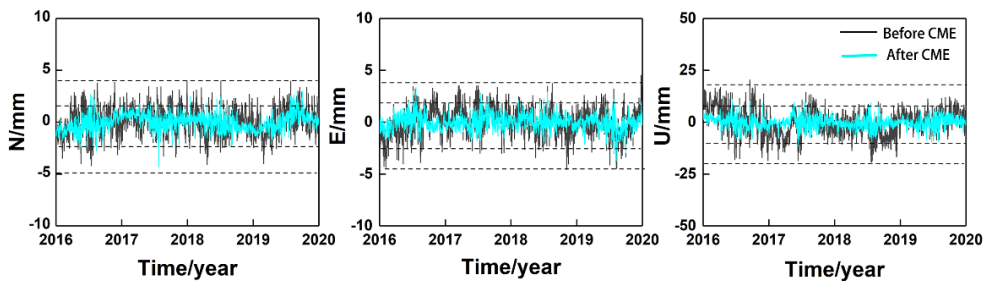


Fig. 4 Residual time series before and after removing CME of SXYC. The dashed line indicates the approximate range of the displacement.

post-processing stage using stacking filtering. We have modified the traditional regional stacking filter method of calculating CME by adding correlation coefficients and distance factors as weights to participate in the calculation of single station CME (Section 2.2.2). Figure 4 shows the residual time series of the station before and after removing the CME.

It can be seen that after removing the CME, the time series in the N, E and U directions all tend to be smooth. Although there are slight fluctuations, the overall magnitude of the fluctuations is reduced, by accounting for the mean of the amount of change, we found that 2mm reduction in amplitude in the N and E and 5mm in the U direction, indicating that the CME can be effectively removed by our improved stacking filter, which in turn enhances the robustness of the coordinate time series. We use the inter-station correlation coefficient and RMS to evaluate the effectiveness of extracting CME. The inter-station correlation coefficient can describe the correlation between the residual time series times of each station,

while the change in RMS can be used to represent the effect of our CME extraction (Li et al., 2018; Percival et al., 2022). Figure 5 shows the RMS statistics of the residual time series before and after CME removal.

As can be seen, before removing the CME, the mean RMS values of the coordinate time series for the N, E and U are 1.71 mm, 1.74 mm and 6.32 mm, respectively, and after the removal of the CME which are reduced to 1.22 mm, 1.21 mm and 3.42 mm, respectively. The average improvements of RMS in the N, E and U directions were 27.8 %, 29.0 %, and 46.0 %. We use the correlation coefficient to characterize the degree of similarity between the time series of different stations. The range of the correlation coefficient is between [0,1], with 0 representing independence and larger values indicating stronger correlation. The CME is a multiple spatial and temporal correlation error set that exists at most stations in the region. After removing the common mode errors, the correlation between the benchmark stations is weakened and the correlation coefficient is

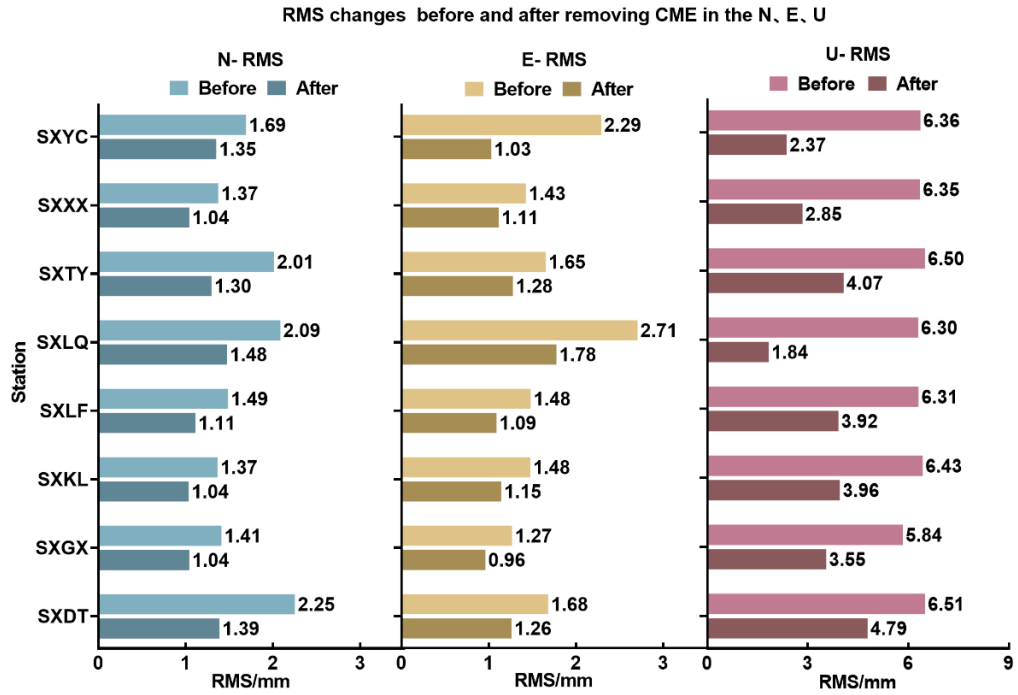


Fig. 5 RMS changes before and after removing the CME in the N, E and U.

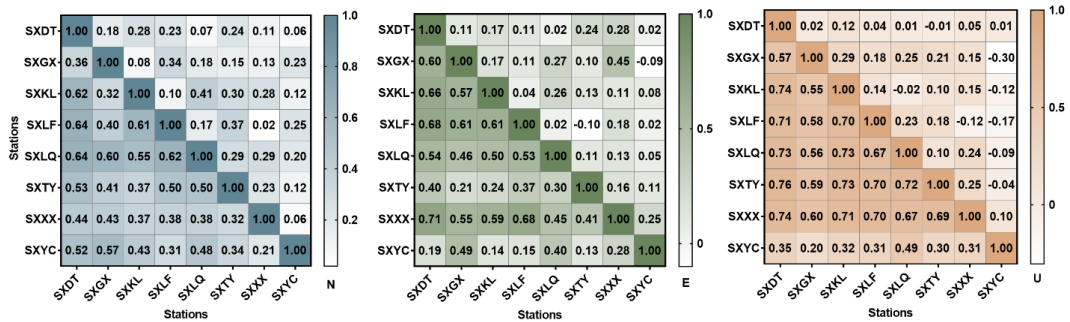


Fig. 6 Interstation correlation coefficients before and after removal of CME from the residual time.

reduced accordingly (Gruszczynski et al., 2016; Zhou et al., 2020, 2022). Figure 6 shows the interstation correlation coefficients before and after removal of CME from the residual time series for the north (left panel), east (middle panel) and up (right panel) components, where the lower triangle indicates the correlation coefficient between stations before CME removal and the upper triangle indicates the correlation coefficient between stations after CME removal. As we can see, after removing the CME, the correlation coefficients present obvious reduction, demonstrating that our improved CME extraction method can effectively remove the "similar parts" between stations.

Meanwhile, in order to verify whether our proposed improved method has a better CME extraction effect compared with the traditional stacking filter, we processed the data by using the two

methods separately, and the RMS comparison of the residual time series of each station after CME extraction using the two methods is given in Table 2.

Meanwhile, in order to verify whether our proposed improved method has a better CME extraction effect compared with the traditional stacking filter, we processed the data by using the two methods separately, and the RMS comparison of the residual time series of each station after CME extraction using the two methods is given in Table 2.

#### 4. DISCUSSION

##### 4.1. THE SPATIAL AND TEMPORAL DISTRIBUTION CHARACTERISTICS OF CME

CME is a spatial correlation error, thus the spatial correlation between stations is intrinsically linked to the spatial distribution of CME. As shown in Figure 5, the correlation coefficient between stations is large

**Table 2** Comparison of RMS after CME extraction using two different methods.

Station	N		E		U	
	Traditional	Improved	Traditional	Improved	Traditional	Improved
SXDT	1.52	1.39	2.05	1.26	5.67	4.79
SXGX	1.55	1.04	1.91	0.96	6.64	3.55
SXKL	1.15	1.04	1.26	1.15	4.58	3.96
SXLF	1.54	1.11	1.24	1.09	4.25	3.92
SXLQ	1.64	1.48	2.18	1.78	4.11	1.84
SXTY	1.52	1.30	0.99	1.28	4.92	4.07
SXXX	1.57	1.04	1.11	1.11	4.99	2.85
SXYC	1.87	1.25	1.31	1.03	3.47	3.37

**Table 3** Correlation coefficient of SXTY with stations at different distances.

Station	Distance (km)	Correlation coefficient		
		N	E	U
SXTY-SXDT	280.3	0.665	0.559	0.440
SXTY-BJFS	367.4	0.447	0.318	0.163
SXTY-WUHN	796.4	0.114	0.012	0.066
SXTY-JFNG	800.8	0.014	0.118	0.000
SXTY-TWTF	1577.6	0.008	0.000	0.007
SXTY-AIRA	1597.2	0.000	0.000	0.015
SXTY-GMSD	1877.5	0.000	-0.172	-0.023
SXTY-SMST	2060.2	-0.003	0.000	0.012
SXTY-URUM	2376.8	0.000	-0.104	-0.003
SXTY-STK2	2385.3	-0.003	0.011	0.035
SXTY-NVSK	2885.2	-0.220	-0.283	0.286
SXTY-CCJ2	2994.1	-0.185	-0.014	-0.130

before the CME is removed, while the correlation between stations is significantly reduced after the CME is removed. Therefore, the correlation coefficient can be used to characterize the degree of correlation between the stations.

While the spatial correlation between the residual coordinate time series of the stations is caused by the environmental factors of the reference stations and the data processing strategy, this correlation gradually decreases as the distance between the reference stations increases. In order to analyse the distribution characteristics of CME in a large regional range, we take SXTY station as a reference and determine correlation coefficients from within 400 km to within 3,000 km. The obtained distances and correlation coefficients (Table 3) show that the overall trend of the correlation coefficients in the N, E, and U directions tend to decrease with increasing distance between stations, while the mean value is gradually approaching zero when the spatial scale reaches 1,600 km. This is consistent with the conclusion from Gong et al. (2016). Interestingly, we found that not all stations follow the inversely proportional rule between the correlation coefficient and distance, and there are cases where the correlation coefficient is close to 0.3 when the stations are far away. This is similar to the finding of Xie et al. (2014), which revealed that a more significant correlation still existed when the distance between some stations exceeded 5,000 km.

Here we draw out the spatial distribution pattern of CME based on the above analysis and previous studies. In the small-scale regional, the correlation between the stations is strong, and the CME in the coordinate time series is approximately uniformly distributed, as the scale increases and the distance between stations increases, the correlation coefficient gradually decreases, and the CME no longer shows the characteristics of uniform distribution, and its spatial distribution is related to the magnitude of the correlation between stations (Gong et al., 2016; Wang et al., 2018).

In addition to the spatial distribution pattern, we also studied the temporal characteristics of the CME. Taking the SXYC station as an example, we extracted the CME time series of the station, as shown in Figure 7.

We find that the magnitude of change in the CME time series is about 3 mm in the N and E directions and about 13 mm in the U direction. The CME time series plots of the remaining stations were similar to those of SXYC station. In order to investigate whether the CME time series are periodic and given that the Fast Fourier Transform is very sensitive to missing data, we chose to use serial correlation to further analyse the periodicity, which is more accurate and less sensitive to missing data. The extremes in Figure 8 are periods, and we can see that there is no obvious periodicity in CME series in the N,

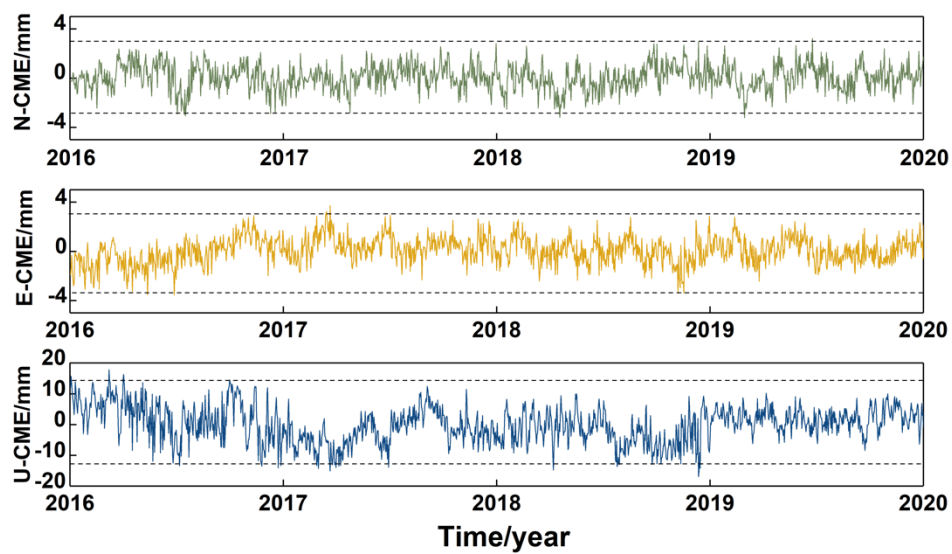


Fig. 7 CME time series of SXYC.

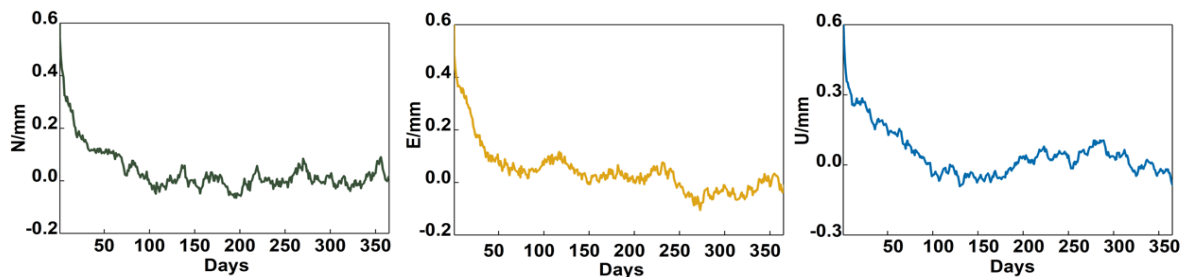


Fig. 8 Autocorrelation function of the CME time series.

E and U directions. We consider that the annual period term in the time series was deducted thoroughly when fitting the raw time series in Section 3.1, resulting in no obvious periodicity in the common part of the residual time series of each station, and Lei et al. (2022) used the independent component method to extract the CME of Xinjiang, and performed ensemble empirical modal decomposition and fast Fourier transform on the CME time series to find that there were annual periodic terms in the CME that were not completely removed in the fit of each station.

#### 4.2. POTENTIAL GEOPHYSICAL INTERPRETATION OF THE CME

In previous studies, many scholars have demonstrated that CME may be related to geophysical factors such as loading including atmospheric pressure loading, hydrological loading, and non-tidal ocean loading (Jiang et al., 2013; Bian et al., 2021; Ma et al., 2021). There are three main aspects of environmentally induced surface deformation: (1) changes in atmospheric loading due to a drop in atmospheric pressure; (2) changes in non-tidal ocean loading due to changes in atmospheric pressure and wind; and (3) increases in land hydrological loading due to heavy rainfall (Yao et al., 2020; He et al.,

2017b). The environmental loading data provided by GFZ, including NTAL, NTOL and HYDL, were chosen. Figure 9 shows the time series of the total environmental loading (average all load series displacements into the daily results) in the U direction at SXYC, from the figure we can see that the amplitude of the environmental loading time series in the U direction is 15 mm.

If the environmental loading series has a similar trend and a degree of correlation with the CME time series, then the amplitude of the CME should decrease after the environmental loading correction. Then the environmental loadings are considered to be one of the potential sources of CME. Table 4 shows the correlation coefficient between environmental loading and CME.

In general, if the absolute value of the correlation coefficient is between 0 and 0.1, it is a negligible correlation, between 0.1 and 0.39 is a weak correlation and between 0.4 and 0.6 means a moderate correlation (Schober et al., 2018). The correlation coefficients in the N and E directions are concentrated but the correlation can be ignored, with average correlation coefficients of -0.002 and 0.013 respectively; in the U direction, there is some correlation, with a maximum correlation coefficient of 0.331 and an average

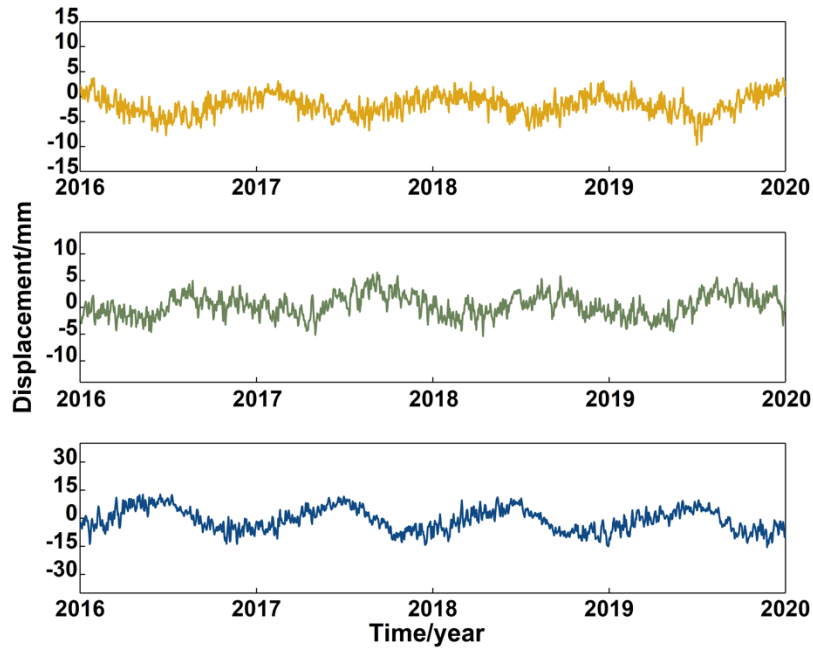


Fig. 9 Loading time series for SXYC.

Table 4 Correlation coefficient between environmental loading and CME.

Station	N	E	U
SXDT	0.0038	0.0074	0.2445
SXGX	-0.0082	0.0187	0.2312
SXKL	0.0026	0.0129	0.3308
SXLF	-0.0074	0.0227	0.2974
SXLQ	-0.0042	0.0035	0.3141
SXTY	-0.0039	0.0133	0.3276
SXXX	0.0059	0.0185	0.2288
SXYC	-0.0056	0.0119	0.3175

correlation coefficient of 0.278, which is generally more evenly distributed. The correlation analysis between environmental loading time series and CME time series indicates that environmental loading has some similarity with the trend of CME series in the U-direction, and environmental load is likely to be one of the causes of CME and possibly be the cause of the vertical deformation in Shanxi. This estimate is consistent with the results obtained by combining GRACE and GPS to compare vertical surface deformation in Shanxi Province by Jiang et al. (2013). We corrected the time series for environmental loading and Figure 10 shows the CME time series before (red) and after (blue) correction for SXYC station. It can be seen that the amplitude of CME before and after the correction in the N and E directions is not obvious, but the amplitude of the CME period term is reduced after the environmental load correction in the U direction, from  $\pm 15$  mm (blue) to  $\pm 13$  mm (red), which is consistent with the results of the study in the Hong Kong, by analyzing time series of 12 stations, suggesting that environmental

loading can explain about 3 mm of the vertical variation in the CME series (Yuan et al., 2013).

In this paper, we are considering NTAL, NTOL and HYDL together to study the effect of environmental loadings on CME, while the effect of different load models on CME in Shanxi can be studied separately in subsequent studies. Previous studies using CME from GNSS data in northwest of Yunnan, and have shown that the combination of HYDL, NTAL and NTOL time series provided by GFZ has better agreement with CME from GPS vertical time series compared to HYDL (Zhang et al., 2020) and non-tidal ocean load vertical deformation is greater than atmospheric load deformation (Yao et al., 2020). On the other hand, hydrological models are also limited by their poor representation of groundwater storage (Riddell et al., 2020). Since we did not have access to groundwater data for this area, we did not consider groundwater, although it is known that extraction and recharge signals can contribute significantly to vertical land movement signals, e.g., in the Perth Basin (Featherstone et al., 2015).

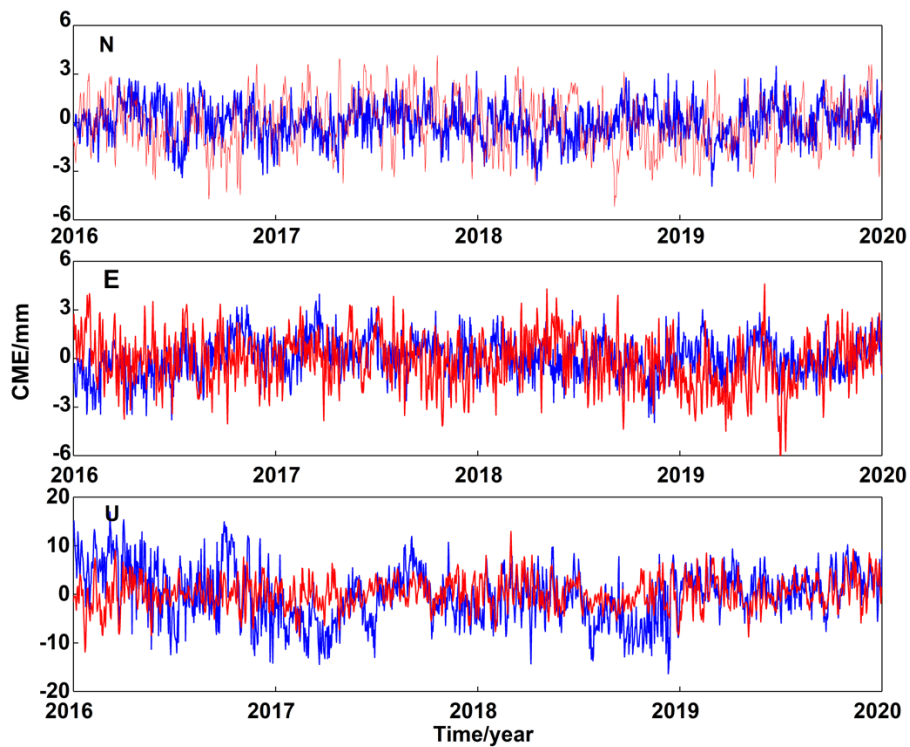


Fig. 10 The CME time series before (red) and after (blue) loading correction for SXYC.

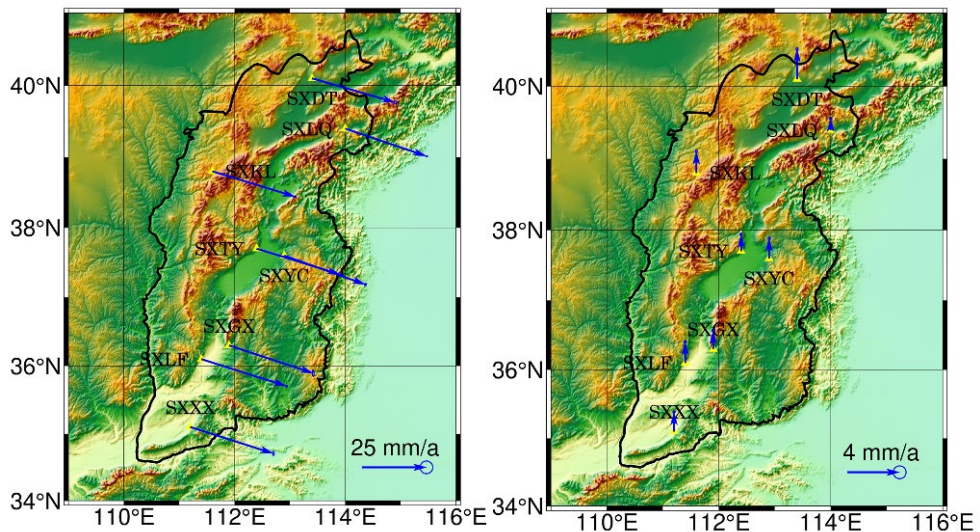


Fig. 11 Velocity field after the CME correction. The left is the horizontal direction and the right is the vertical direction.

Hydrological loading could be studied accordingly in subsequent studies in conjunction with gravity recovery and climate experiment (GRACE) and interferometric synthetic aperture radar (InSAR) (Tang et al., 2018; Li et al., 2022).

#### 4.3. EFFECTS OF CME ON GPS TIME SERIES

To further explore the effect of CME on GPS time series, we investigated the effect of CME on the velocity estimation and the noise component

separately. Figure 11 shows the horizontal and vertical velocity fields of the stations after the CME correction. The Shanxi region in general shows a near-SE directional motion, with an average rate of 33 mm/a in the corrected horizontal direction, and in the vertical direction, the maximum uplift is SXKL, which reaches 3.5 mm/a, this is consistent with previous studies in this area (Cheng et al., 2021).

The velocities in the N direction at all stations are in the range of 9-12 mm/a, and the velocities in the E

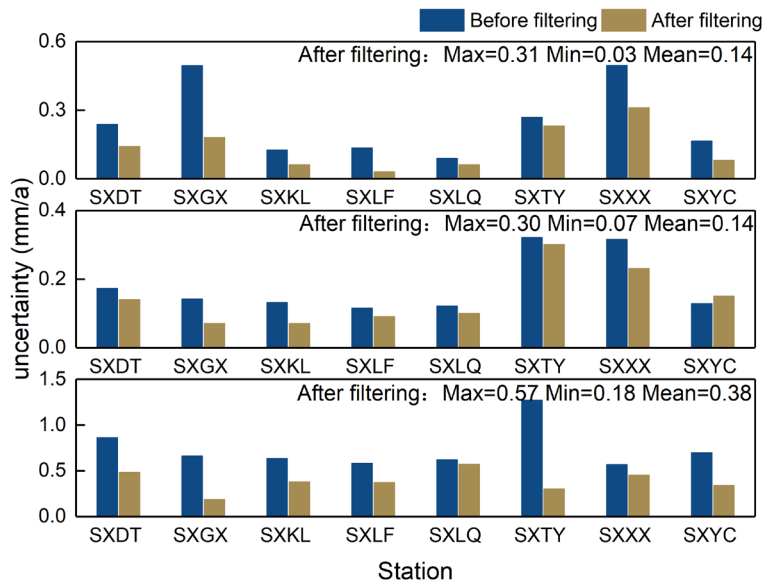


Fig. 12 Change in velocity uncertainty before and after CME removal.

Table 5 Spectral indices of the stations in the N, E and U.

Station	N	E	U
SXDT	-1.33	-1.11	-0.83
SXGX	-1.12	-1.39	-0.62
SXKL	-0.96	-1.06	-0.75
SXLF	-1.37	-1.13	-0.82
SXLQ	-1.18	-1.29	-0.71
SXTY	-1.25	-1.20	-0.68
SXXX	-1.16	-1.32	-0.63
SXYC	-1.37	-1.17	-0.58

direction are in the range of 31-34 mm/a. The difference between stations is less than 3 mm/a, indicating a relatively uniform spatial distribution of horizontal velocities. Figure 12 shows the change of velocity uncertainty before and after filtering. Before CME correction, the mean velocity uncertainties in the N, E and U directions were 0.25 mm/a, 0.18 mm/a and 0.74 mm/a, respectively. After CME correction, they were reduced by 46.28 %, 21.40 % and 43.65 % respectively. This proves that the removal of CME can reduce the uncertainty of the station time series and thus improve the reliability of the GNSS coordinates.

Meanwhile, we conducted a noise analysis of the time series. Using the spectral index estimation method, the spectral index of the coordinate directional components of each station can be obtained, thus roughly determining the type of noise. Williams et al. (2004) analyzed 414 sites. Using spectral index analysis of power law noise models for SOPAC global solutions, they summarized that 96.6 % of them could be described by white noise plus flicker noise. In this section, we use the spectral index analysis in section 2.2.3 to perform noise analysis on the Shanxi Province data, Table 5 shows the results of

the spectral indices for each station on the three components N, E and U. It can be seen that the spectral indices on the N, E and U components are all between [-2,0], indicating that the components contain not only white noise but also contains coloured noise.

From the results in Table 5, we can then approximately determine that the data studied in this paper is dominated by white noise and scintillation noise. For further verification and obtain the optimal noise model, we use five noise models of Hector software to solve the data of the three directional components of the eight stations, and the optimal noise model for the stations in Shanxi Province was obtained by using the BIC analysis method based on maximum likelihood estimation, the results of the optimal noise models in the N, E and U directions for all stations as a percentage (%) are shown in Table 6. From the results of the BIC analysis, it can be learned that for most of the stations in Shanxi, flicker noise (FN) + white noise (WN) is the optimal noise model, and for a small number of stations, power-law noise (PL) + white noise (WN) is a better noise model. This is consistent with previous studies that white noise plus flicker noise is generally preferable to white noise plus

**Table 6** Proportion of the optimal noise model of N, E and U.

Dir	PL+WN		FN+WN		GGM+WN	
	Before	After	Before	After	Before	After
N	20 %	20 %	80 %	70 %	0 %	10 %
E	30 %	20 %	70 %	80 %	0 %	0 %
U	30 %	30 %	70 %	60 %	0 %	0 %

**Table 7** Change in noise component before and after removal of CME.

Station	Dir	WN			FN			RWN		
		Before (mm)	After (mm)	Percentage* (%)	Before (mm)	After (mm)	Percentage* (%)	Before (mm)	After (mm)	Percentage* (%)
SXDT	N	0.68	0.56	+17.65	3.47	2.03	+41.50	0.00	0.00	0.00
	E	0.85	0.74	+12.94	2.41	1.73	+28.22	4.51	3.82	+15.30
	U	2.70	1.65	+38.89	15.99	6.57	+58.91	3.23	1.91	+40.87
SXGX	N	0.99	0.62	+37.37	2.66	1.80	+32.33	1.43	1.64	-14.69
	E	0.91	0.80	+12.09	3.09	2.08	+32.69	2.41	2.54	-5.39
	U	3.23	2.48	+23.22	17.65	8.07	+54.28	0.00	0.00	0.00
SXXL	N	0.62	0.44	+29.03	3.88	2.30	+40.72	0.00	0.00	0.00
	E	0.70	0.47	+32.86	3.00	2.02	+32.67	1.31	1.50	-14.50
	U	2.65	1.76	+33.58	15.67	8.01	+48.88	0.00	0.00	0.00
SXLF	N	0.78	0.52	+33.33	2.87	1.90	+33.80	0.00	0.00	0.00
	E	0.86	0.50	+41.86	2.78	1.74	+37.41	1.97	2.05	-4.06
	U	3.09	2.26	+26.86	15.35	6.36	+58.57	0.00	0.00	0.00
SXLQ	N	0.90	0.66	+26.67	3.23	2.04	+36.84	0.00	0.00	0.00
	E	0.88	0.67	+23.86	2.69	1.46	+45.72	0.00	2.42	0.00
	U	2.99	1.75	+41.47	16.73	9.02	+46.08	0.00	4.37	0.00
SXTY	N	0.73	0.45	+38.36	4.91	2.74	+44.20	2.32	1.20	+48.28
	E	0.87	0.64	+26.44	5.27	3.77	+28.46	0.00	0.00	0.00
	U	2.80	1.55	+44.64	16.19	8.67	+46.45	0.00	0.00	0.00
SXXX	N	0.81	0.56	+30.86	3.19	1.26	+60.50	2.63	1.76	+33.08
	E	0.94	0.68	+27.66	2.86	1.74	+39.16	2.79	2.93	-5.02
	U	3.45	1.95	+43.48	14.71	6.97	+52.62	0.00	0.00	0.00
SXYC	N	0.75	0.55	+26.67	3.04	1.74	+42.76	0.00	0.00	0.00
	E	0.79	0.53	+32.91	2.92	1.93	+33.90	1.14	1.11	+2.63
	U	2.98	2.24	+24.83	15.79	6.54	+58.58	0.00	0.00	0.00

\*: '+' indicates RMS decrease after filtering; '-' indicates RMS increase after filtering.

random walk noise or WN model in GPS position time series (Zhang et al., 1997; Mao et al., 1999; Williams et al., 2004).

To investigate the effect of CME on the time series noise analysis in Shanxi Province, the time series noise analysis after removing the CME was re-analyzed using BIC analysis and compared with the noise analysis results before removing the CME. The comparative results of the BIC numerical analysis are shown in Table 6. The results of each noise component in N, E and U directions before and after removing the CME are shown in Table 7.

It can be seen that the noise levels have been significantly reduced after filtering, with WN, FN and RWN being reduced by 30.31 %, 43.14 % and 4.02 % respectively. It is inferred that the flicker noise dominates the CME component in Shanxi. In other words, the CME in Shanxi has a mixture of WN and

FN. This echoes Li's research, in which he indicates that a significant amount of the colored noise in the unfiltered time series is attributed to the common physical basis with some spatial extent, such as common mode signature (Li et al., 2018).

## 5. CONCLUSION

This study used the raw coordinate time series data of eight continuously observed reference stations in Shanxi Province from 2016-2020. The trend term and period terms (annual and semi-annual) was removed to obtain the residual time series, then we extracted the CME using our proposed improved stacking filtering method and verified its extraction effect, and finally performed the analysis on the time series before and after removing the CME to obtain the following observation.

This study improved the stacking filter method by considering the correlation coefficient and distance factor (spherical distance between stations), and compared with the traditional method. Our results showed that the improved stacking filter method could extract CME more accurately.

Environmental loading may be one of the main sources of CME in the vertical direction. CME correction of the time series can make the estimated velocities and their uncertainties more accurate, which is important for the study of tectonic motion.

The noise analysis of the time series was carried out using the spectral index estimation and BIC analysis, and the noise models of the coordinate time series of the stations were found to be dominated by flicker noise (FN) + white noise (WN). It is also found that while power-law noise (PL) + white noise (WN), and random walk noise (RWN) also existed in some stations. The optimal noise model for Shanxi is FN + WN. After removing the CME, the magnitude of each noise component drops significantly, with the largest dropping of FN by 56.76 %, indicating that the CME contains a large amount of noise, especially flicker noise, which confirmed the importance of removing the CME.

#### ACKNOWLEDGMENTS

We acknowledge the GNSS Data Product Service Platform of the China Seismological Bureau (<http://www.cgps.ac.cn>) for data support in Shanxi Province. Bos et al. (2013) for developing the time series analysis software Hector. Some of the figures were plotted using the Generic Mapping Tools (GMT) software, developed by Wessel and Smith (1991). The research was funded by National Natural Science Foundation of China (41861061, 41930101, 42204006), China Postdoctoral Science Foundation (2019M660091XB), Gansu Higher Education Innovation and Promotion Project (2020A-037), Key Laboratory of Geography and National Condition Monitoring, Ministry of Natural Resources (2022NGCM01), the Open Research Fund Program of the National Cryosphere Desert Data Center (E01Z790201/2021kf07), Natural Science Foundation of Gansu Province (20JR10RA271, 21JR7RA317), “Young Scientific and Technological Talents Lifting Project” Project of Gansu Province in 2020 (Li Wei), “Tianyou Youth Lifting Project” Program of Lanzhou Jiaotong University (Li Wei), Innovation and Entrepreneurship Education Reform and Cultivation Project in Gansu Province (1A50190117).

#### REFERENCES

- Abdi, H. and Williams, L.: 2010, Principal component analysis. *Wiley Interdiscip. Rev.: Comput. Stat.*, 2, 4, 433–459. DOI: 10.1002/wics.101
- Altamimi, Z., Rebischung, P., Métivier, L. and Collilieux, X.: 2016, ITRF2014: A new release of the international terrestrial reference frame modeling nonlinear station motions. *J. Geophys. Res., Solid Earth*, 121, 8, 6109–6131. DOI: 10.1002/2016JB013098
- Arnosó, J., Riccardi, U., Benavent, M., Tammaro, U. and Vélez, E.: 2020, Strain pattern and kinematics of the Canary Islands from GNSS time series analysis. *Remote Sens.*, 12, 20, 3297. DOI: 10.3390/rs12203297
- Barani, S., Cristofaro, L., Taroni, M., Gil-Alaña, L. A. and Ferretti, G.: 2021, Long memory in earthquake time series: The case study of the geysers geothermal field. *Front. Earth Sci.*, 9, 563649. DOI: 10.3389/feart.2021.563649
- Bian, Y., Yue, J., Ferreira, V. G., Cong, K. and Cai, D.: 2021, Common mode component and its potential effect on GPS-inferred crustal deformations in Greenland. *Pure Appl. Geophys.*, 178, 5, 1805–1823. DOI: 10.1007/s00024-021-02732-z
- Blewitt, G. and Lavallée, D.: 2002, Effect of annual signals on geodetic velocity. *J. Geophys. Res., Solid Earth*, 107, B7, ETG-9. DOI: 10.1029/2001JB000570
- Bogusz, J., Klos, A. and Pokonieczny, K.: 2019, Optimal strategy of a GPS position time series analysis for post-glacial rebound investigation in Europe. *Remote Sens.*, 11, 1209. DOI: 10.3390/rs11101209
- Bos, M.S., Fernandes, R., Williams, S. and Bastos, L.: 2013, Fast error analysis of continuous GNSS observations with missing data. *J. Geod.*, 87, 4, 351–360. DOI: 10.1007/s00190-012-0605-0
- Cheng, C., Li, Y. and Ping, Q.: 2021, Time series analysis of GNSS base station in Shanxi province. *Earthquake Research in Shanxi*, 3, 25–29. DOI: 10.3969/j.issn.1000-6265.2021.04.008
- Ding, K., Freymueller, J.T., He, P., Wang, Q. and Xu, C.: 2019, Glacial isostatic adjustment, intraplate strain, and relative sea level changes in the eastern United States. *J. Geophys. Res., Solid Earth*, 124, 6, 6056–6071. DOI: 10.1029/2018JB017060
- Dmitrieva, K., Segall, P. and Demets, C.: 2015, Network-based estimation of time-dependent noise in GPS position time series. *J. Geod.*, 89, 6, 591–606. DOI: 10.1007/s00190-015-0801-9
- Dong, D., Fang, P., Bock, Y., Webb, F., Prawirodirdjo, L., Kedar, S. and Jameson, P.: 2006, Spatiotemporal filtering using principal component analysis and Karhunen-Loeve expansion approaches for regional GPS network analysis. *J. Geophys. Res., Solid Earth*, 111, B3. DOI: 10.1029/2005JB003806
- Fernandes, R., He, X., Montillet, J.P., Bos, M., Melbourne, T., Jiang, W. and Zhou, F.: 2020, Spatial variations of stochastic noise properties of GNSS time series. EGU General Assembly Conference Abstracts, EGU2020-21260. DOI: 10.5194/egusphere-egu2020-21260
- Featherstone, W., Penna, N., Filmer, M. and Williams, S.: 2015, Nonlinear subsidence at Fremantle, a long-recording tide gauge in the Southern Hemisphere. *J. Geophys. Res., Oceans*, 120, 10, 7004–7014. DOI: 10.1029/2019JB018034
- Gruszczynski, M., Klos, A. and Bogusz, J.: 2016, Orthogonal transformation in extracting of common mode errors from continuous GPS networks. *Acta Geodyn. Geomater.*, 13, 3, 291–298. DOI: 10.13168/AGG.2016.0011
- He, X., Bos, M., Montillet, J. and Fernandes, R.: 2019, Investigation of the noise properties at low frequencies in long GNSS time series. *J. Geod.*, 93, 1271–1282. DOI: 10.1007/s00190-019-01244-y
- He, X., Hua, X., Yu, K., Xuan, W., Lu, T., Zhang, W. and Chen, X.: 2015, Accuracy enhancement of GPS time series using principal component analysis and block

- spatial filtering. *Adv. Space Res.*, 55, 5, 1316–1327. DOI: 10.1016/j.asr.2014.12.016
- He, X., Montillet, J.P., Fernandes, R., Bos, M., Yu, K., Hua, X. and Jiang, W.: 2017a, Review of current GPS methodologies for producing accurate time series and their error sources. *J. Geodyn.*, 106, 12–29. DOI: 10.1016/j.jog.2017.01.004
- He, X., Montillet, J.P., Hua, X., Yu, K., Jiang, W. and Zhou, F.: 2017b, Noise analysis for environmental loading effect on GPS position time series. *Acta Geodyn. Geomater.*, 14, 1, 131–142. DOI: 10.13168/AGG.2016.0034
- Hein, G.: 2020, Status, perspectives and trends of satellite navigation. *Satell. Navig.*, 1, 1, 1–12. DOI: 10.1186/s43020-020-00023-x
- Herring, T.: 2003, MATLAB Tools for viewing GPS velocities and time series. *GPS Solut.*, 7, 3, 194–199. DOI: 10.1007/s10291-003-0068-0
- Herring, T., King, R. and McClusky, S., 2010. *Introduction to GAMIT*. Massachusetts Institute of Technology, Cambridge, Massachusetts.
- Iqbal, R., Syafriani, Arisa, D. and Setiadi, B.: 2021, Deformation analysis for Padang earthquake using GPS data. *J. Phys. Conf. Ser.*, 1876, 1, 012029. DOI: 10.1088/1742-6596/1876/1/012029
- Jackson, D. and Yong, C.: 2004, Robust principal component analysis and outlier detection with ecological data. *Environmetrics*, 15, 2, 129–139. DOI: 10.1002/env.628
- Ji, K. and Herring, T.A.: 2013, A method for detecting transient signals in GPS position time-series: smoothing and principal component analysis. *Geophys. J. Int.*, 193, 1, 171–186. DOI: 10.1093/gji/ggt003
- Jiang, W., Li, Z., Liu, H. and Zhao, Q.: 2013, Cause analysis of the non-linear variation of the IGS reference station coordinate time series inside China. *Chin. J. Geophys.*, 56, 4, 2228–2237, (in Chinese). DOI: 10.1002/cjg2.20033
- Jiang, W., Ma, Y. and Deng, L.: 2016, Establishment of mm-level terrestrial reference frame and its prospect. *J. Geomat.*, 41, 4, 1–6, (in Chinese). DOI: 10.1038/s41598-017-06095-1
- Jiang, W., Yuan, P., Chen, H., Cai, J., Li, Z., Chao, N. and Sneeuw, N.: 2017, Annual variations of monsoon and drought detected by GPS: A case study in Yunnan, China. *Sci. Rep.*, 7, 1, 1–10. DOI: 10.1038/s41598-017-06095-1
- Jiang, W., Wang, K., Li, Zhao., Zhou, X., Ma, Y. and Ma J.: 2018, Prospect and theory of GNSS coordinate time series analysis. *Geomat. Inform. Sci. Wuhan Univ.*, 43, 12, 2112–2123, (in Chinese). DOI: 10.13203/j.whugis20180333
- Langbein, J.: 2004, Noise in two-color electronic distance meter measurements revisited. *J. Geophys. Res., Solid Earth*, 109, B4. DOI: 10.1029/2003JB002741
- Langbein, J.: 2012, Estimating rate uncertainty with maximum likelihood: differences between power-law and flicker-random-walk models. *J. Geod.*, 86, 9, 775–783. DOI: 10.1007/s00190-012-0556-5
- Lei, C., Wei, G., Gao, M. and Zhang P.: 2022, Analysis of common mode error of GNSS coordinate time series in Xinjiang with independent component analysis. *GNSS World of China*, 47, 3, 1–8, (in Chinese). DOI: 10.12265/j.gnss.2021111201
- Li, W., Dong, J., Wang, W., Zhong, Y., Zhang, C., Wen, H., Liu, H., Guo Q. and Yao, G.: 2022, The crustal vertical deformation driven by terrestrial water load from 2010 to 2014 in Shaanxi–Gansu–Ningxia region based on GRACE and GNSS. *Water*, 14, 6, 964. DOI: 10.3390/w14060964
- Li, W., Jiang, W., Li, Z., Chen, H., Chen, Q., Wang, J. and Zhu, G.: 2020, Extracting common mode errors of regional GNSS position time series in the presence of missing data by variational Bayesian principal component analysis. *Sensors*, 20, 8. DOI: 10.3390/s20082298
- Li, W., Li, Z., Jiang, W., Chen, Q., Zhu, G. and Wang, J., 2022. A new spatial filtering algorithm for noisy and missing GNSS position time series using Weighted Expectation Maximization Principal Component Analysis: A case study for regional GNSS network in Xinjiang Province. *Remote Sens.*, 14, 5, 1295. DOI: 10.3390/rs14051295
- Li, Q., Ning, B., Zhao, B., Ding, F., Zhang, R., Shi, H., Yue, H., Li, G., Li, J. and Han, Y.: 2012, Applications of the CMONOC based GNSS data in monitoring and investigation of ionospheric space weather. *Chin. J. Geophys.*, 55, 7, 2193–2202, (in Chinese). DOI: 10.6038/j.issn.0001-5733.2012.07.006
- Li, Y.: 2021, Analysis of GAMIT/GLOBK in high-precision GNSS data processing for crustal deformation. *Earthq. Res. Adv.*, 1, 3, 1–9. DOI: 10.1016/j.eqrea.2021.100028
- Li, Y., Xu, C., Yi, L. and Fang, R.: 2018, A data-driven approach for denoising GNSS position time series. *J. Geod.*, 92, 8, 905–922. DOI: 10.1007/s00190-017-1102-2
- Liu, N., Dai, W., Santerre, R. and Kuang, C.: 2018, A MATLAB-based Kriged Kalman Filter software for interpolating missing data in GNSS coordinate time series. *GPS Solut.*, 22, 1, 1–8. DOI: 10.1007/s10291-017-0689-3
- Lu, X., Jiang, L., Xiao, C. and Li, D.: 2022, Analyzing spatial-temporal variability of ice motion in northeast Greenland from 1985 to 2018. *Front. Earth Sci.*, 10, 972291. DOI: 10.3389/feart.2022.972291
- Ma, X., Liu, B., Dai, W., Kuang, C. and Xing, X.: 2021, Potential contributors to common mode error in array GPS displacement fields in Taiwan Island. *Remote Sens.*, 13, 21, 4221. DOI: 10.3390/rs13214221
- Mao, A., Harrison, C. and Dixon, T.: 1999, Noise in GPS coordinate time series. *J. Geophys. Res., Solid Earth*, 104, B2, 2797–2816. DOI: 10.1029/1998JB900033
- Ming, F., Yang, Y., Zeng, A. and Zhao, B.: 2017, Spatiotemporal filtering for regional GPS network in China using independent component analysis. *J. Geod.*, 91, 4, 419–440. DOI: 10.1007/s00190-016-0973-y
- Montillet, J., Tregoning, P., McClusky, S. and Yu, K.: 2012, Extracting white noise statistics in GPS coordinate time series. *IEEE Geosci. Remote Sens. Lett.*, 10, 3, 563–567. DOI: 10.1109/LGRS.2012.2213576
- Nikolaidis, R.: 2002, Observation of geodetic and seismic deformation with the Global Positioning System, PhD thesis, University of California, San. Diego.
- Percival, J.E.H., Tsutsumida, N., Murakami, D., Yoshida, T. and Nakaya, T.: 2022, Exploratory spatial data analysis with gwpcorMapper: an interactive mapping tool for geographically weighted correlation and partial correlation. *J. Geovis. Spat. Anal.*, 6, 1, 17. DOI: 10.1007/s41651-022-00111-3

- Qiu, X., Wang, F., Zhou, Y. and Zhou, S.: 2022, Iteration empirical mode decomposition method for filling the missing data of GNSS position time series. *Acta Geodyn. Geomater.*, 19, 4, 271–279. DOI: 10.13168/AGG.2022.0012
- Riddell, A., King, M. and Watson, C.: 2020, Present-day vertical land motion of Australia from GPS observations and geophysical models. *J. Geophys. Res., Solid Earth*, 125, 2, e2019JB018034. DOI: 10.1029/2019JB018034
- Schober, P., Boer, C. and Schwarte, L.A.: 2018, Correlation coefficients: appropriate use and interpretation. *Anesth. Analg.*, 126, 5, 1763–1768. DOI: 10.1213/ANE.0000000000002864
- Sheng, C., Gan, W., Liang, S., Chen, W. and Xiao, G.: 2014, GRACE discrimination and rejection of terrestrial water load deformation disturbances in GPS time series in western Yunnan. *J. Geophys.*, 1, 42–52, (in Chinese). DOI: 10.6038/cjg20140105
- Sui, Z., Li, J., Wang, S. and Gao, Z.: 2022, Noise and velocity field analysis of Shanxi CMONOC coordinate time series. *Geod. Geodyn.*, 42, 2, 148–152, (in Chinese).
- Tan, W., Chen, J., Dong, D., Qu, W. and Xu, X.: 2020, Analysis of the potential contributors to common mode error in Chuanidian region of China. *Remote Sens.*, 12, 5, 751. DOI: 10.3390/rs12050751
- Tang, W., Yuan, P., Liao, M. and Balz, T., 2018. Investigation of ground deformation in Taiyuan Basin, China from 2003 to 2010, with atmosphere-corrected time series InSAR. *Remote Sens.*, 10, 9, 1499. DOI: 10.3390/rs10091499
- Tian, Y., and Shen, Z.: 2016, Extracting the regional common-mode component of GPS station position time series from dense continuous network. *J. Geophys. Res., Solid Earth*, 121, 2, 1080–1096. DOI: 10.1002/2015JB012253
- Tregoning, P. and Watson, C.: 2009, Atmospheric effects and spurious signals in GPS analyses. *J. Geophys. Res., Solid Earth*, 114, B9. DOI: 10.1029/2009JB006344
- Trubienko, O., Fleitout, L., Garaud, J. and Vigny, C.: 2013, Interpretation of interseismic deformations and the seismic cycle associated with large subduction earthquakes. *Tectonophysics*, 589, 126–141. DOI: 10.1016/j.tecto.2012.12.027
- Wang, J., Zhou, X. and Zhu, Z.: 2018, Research on elimination of common mode error in large-scale GPS networks. *Geod. Geodyn.*, 38, 1, 78–82, (in Chinese). DOI: 10.14075/j.jgg.2018.01.017
- Wdowinski, S., Bock, Y., Fang, P., Zhang, J. and Genrich, J.: 1997, Southern California permanent GPS geodetic array: Spatial filtering of daily positions for estimating coseismic and postseismic displacements induced by the 1992 Landers earthquake. *J. Geophys. Res., Solid Earth*, 102, B8, 18057–18070. DOI: 10.1029/97JB01378
- White, A., Gardner, W., Borsa, A., Argus, D. and Martens, H.: 2022, A review of GNSS/GPS in hydrogeodesy: Hydrologic loading applications and their implications for water resource research. *Water Resour. Res.*, 58, 7, e2022WR032078. DOI: 10.1029/2022WR032078
- Williams, S., Bock, Y., Fang, P., Jamason, P., Nikolaidis, R., Prawirodirdjo, L. and Johnson, D.: 2004, Error analysis of continuous GPS position time series. *J. Geophys. Res., Solid Earth*, 109, B3. DOI: 10.1029/2003JB002741
- Xie, S., Pan, P. and Zhou, X.: 2014, Research on common mode error extraction method for large-scale GPS network. *Geomat. Inform. Sci. Wuhan Univ.*, 39, 10, 1168–1173, (in Chinese). DOI: 10.13203/j.whugis20130565
- Xu, C., Liu, Y., Wen, Y., and Wang, R.: 2010, Coseismic slip distribution of the 2008 Mw 7.9 Wenchuan earthquake from joint inversion of GPS and InSAR data. *Bull. Seism. Soc. Am.*, 100, 5B, 2736–2749. DOI: 10.1785/0120090253
- Yadav, R., Kundu, B., Gahalaut, K., Catherine, J., Gahalaut, V., Ambikaphy, A. and Naidu, M.: 2013, Coseismic offsets due to the 11 April 2012 Indian Ocean earthquakes (Mw 8.6 and 8.2) derived from GPS measurements. *Geophys. Res. Lett.*, 40, 3389–3393. DOI: 10.1002/grl.50601
- Yang, W., Feng, Y., Wan, J. and Wang L.: 2022, Sparse Gaussian process regression for landslide displacement time-series forecasting. *Front. Earth Sci.*, 10, 944301. DOI: 10.3389/feart.2022.944301
- Yuan, G., Ding, X., Chen, W., Kwok, S., Chan, S., Hung, P. and Chau, K.: 2013, Characteristics of daily position time series from the Hong Kong GPS fiducial network. *Chin. J. Geophys.*, 51, 5, 976–990, (in Chinese). DOI: 10.1002/cjg2.1292
- Zhang, Y., Bi, G., Cheng, H. and Feng, Y.: 2012, Research on noise characteristics of time series of CORS sites coordinates in Shanxi Region. *Geod. Geodyn.*, 32, 4, 61–66, (in Chinese). DOI: 10.3969/j.issn.1671-5942.2012.04.014
- Zhang, J., Bock, Y., Johnson, H., Fang, P., Williams, S., Genrich, J. and Behr, J.: 1997, Southern California permanent GPS geodetic array: Error analysis of daily position estimates and site velocities. *J. Geophys. Res., Solid Earth*, 102, B8, 18035–18055. DOI: 10.1029/97JB01380
- Zhang, K., Wang, Y., Gan, W. and Liang, S.: 2020, Impacts of local effects and surface loads on the common mode error filtering in continuous GPS measurements in the northwest of Yunnan province, China. *Sensors*, 20, 18, 5408. DOI: 10.3390/s20185408
- Zhou, W., Ding, K., Liu, P., Lan, G. and Ming, Z.: 2022, Spatiotemporal filtering for continuous GPS coordinate time series in mainland China by using independent component analysis. *Remote Sens.*, 14, 12, 2904. DOI: 10.3390/rs14122904
- Zhou, M., Guo, J., Liu, X., Shen, Y. and Zhao, C.: 2020, Crustal movement derived by GNSS technique considering common mode error with MSSA. *Adv. Space Res.*, 66, 8, 1819–1828. DOI: 10.1016/j.asr.2020.06.018
- Zhou, M., Guo, J., Shen, Y., Kong, Q. and Yuan, J.: 2018, Extraction of common mode errors of GNSS coordinate time series based on multi-channel singular spectrum analysis. *Chin. J. Geophys.*, 61, 4383–4395, (in Chinese). DOI: 10.6038/cjg2018L0710